Proceedings of the Ninth Pacific Conference on Earthquake Engineering
Building an Earthquake-Resilient Society
14-16 April, 2011, Auckland, New Zealand

Developing fragilities for mainshock-damaged structures through incremental dynamic analysis

H. Ryu

University of Colorado at Boulder, Boulder, CO USA. (now Geoscience Australia, Canberra, ACT Australia)

N. Luco

US Geological Survey, Golden, CO USA.

S. R. Uma

GNS Science, Avalon, Lower Hutt, New Zealand.

A. B. Liel

University of Colorado at Boulder, Boulder, CO USA.

ABSTRACT: We present a methodology for developing fragilities for mainshock-damaged structures, "aftershock fragility", by performing incremental dynamic analysis (IDA) with a sequence of mainshock-aftershock ground motions. The aftershock fragility herein is distinguished from a conventional fragility for an intact structure. We estimate seismic response of a mainshock-damaged building by performing nonlinear time history analysis with a sequence of mainshock and aftershock ground motions (so-called "back-to-back" dynamic analysis). We perform the back-to-back dynamic analyses for a number of levels of mainshock response/damage, and a number of sequences of mainshock and aftershock ground motions. With estimated seismic responses from the back-to-back dynamic analyses, we compute various damage state transition probabilities, the probability of exceeding a higher damage state from an aftershock given a damage state due to a mainshock. For an illustration of the methodology, we develop an aftershock fragility for a typical New Zealand 5-storey reinforced concrete moment frame building. The building is modeled using a single-degree-of-freedom (SDOF) damped nonlinear oscillator with force-deformation behavior represented by a multi-linear capacity/pushover curve with moderate pinching hysteresis and medium cyclic deterioration.

1 INTRODUCTION

Most of current seismic risk assessment tools consider risk due to a mainshock event only. However, it is common to observe many aftershocks following the mainshock event, some of which could be strong enough to cause further damage to the building and even loss of human life. After a major earthquake, structural engineers must assess whether damaged buildings can continue to be occupied or not, with due consideration to the threat of aftershocks. An objective and quantifiable criterion that can be used to green/yellow/red-tag a damaged building (within a specified time period) is the probability of collapse in an aftershock. The probability of collapse in an aftershock can be computed by coupling the fragility of mainshock-damaged building with the aftershock ground motion hazard at the location.

Luco et al., (2004) proposed a methodology to compute the residual capacity of a mainshock-damaged building, which could be adopted to develop a fragility for a mainshock-damaged building. In the methodology, the residual capacity of a building in a given post-mainshock damage state is defined as

the smallest ground motion spectral acceleration that would induce localized or complete collapse in an aftershock. Each of five post-mainshock damage states is defined by a deterministic value of peak roof drift. For each realization of a mainshock-damaged building, residual capacities are computed by performing incremental dynamic analysis with aftershock records. There are two major limitations in this methodology: 1) the post-mainshock response given the post-mainshock damage state was assumed to be deterministic; 2) the damage state threshold was assumed to be deterministic.

In this study, we present a methodology for developing fragilities for mainshock-damaged structures, "aftershock fragilities", by performing incremental dynamic analysis (IDA) with a sequence of mainshock-aftershock ground motions. More specifically, we estimate seismic response of a mainshock-damaged building by performing nonlinear time history analysis with a sequence of mainshock and aftershock ground motions (so-called "back-to-back" dynamic analyses). We perform the back-to-back dynamic analyses for a number of levels of mainshock response/damage, and a number of sequences of mainshock and aftershock ground motions. With estimated seismic responses from the back-to-back dynamic analyses, we compute various damage state transition probabilities, the probability of exceeding a higher damage state in an aftershock given a damage state caused by a mainshock. For an illustration of the methodology, we develop an aftershock fragility for a typical New Zealand 5-storey reinforced concrete moment frame building. The building is modeled using a single-degree-of-freedom (SDOF) damped nonlinear oscillator with force-deformation behavior represented by a multi-linear capacity/pushover curve with moderate pinching hysteresis and medium cyclic deterioration.

2 METHODOLOGY

In this section, we present the methodology for developing fragilities for a mainshock-damaged building. We first describe how fragility curves for an intact building are developed, and then describe the methodology for developing fragilities for a mainshock-damaged building.

2.1 Fragility for intact building

A building fragility curve defines the probability that a building experiences a certain damage state or worse, as a function of ground motion intensity. Fragility curves can be computed following Equation 1:

$$P(DS \geq ds \mid IM = im) = \int P(DS \geq ds \mid EDP = edp) \times f(EDP = edp \mid IM = im) dedp \quad (1)$$

where *DS* denotes damage state (e.g., slight), *IM* denotes ground motion intensity (e.g, spectral acceleration), and *EDP* denotes engineering demand parameter (e.g., drift). The first term in Equation 1, $P(DS \geq ds \mid EDP = edp)$, represents the probability of being in or exceeding a damage state, *ds*, given *edp*, and can be computed as

$$P(DS \geq ds \mid EDP = edp) = P(DST_{ds} \leq edp) \quad (2)$$

where DST_{ds} represents the damage state threshold (or capacity). The second term, $f(edp \mid im)$, represents the probability distribution of engineering demands on the structure for a specified ground motion intensity level and can be computed using the results of dynamic analysis of the building under a large number of ground motion records (e.g., incremental dynamic analyses).

Equation 1 can be rewritten as shown in Equation 3:

$$P(DS \geq ds \mid IM = im) = \int P(IM_{ds} \leq im \mid DST_{ds} = edp) \times f(DST_{ds} = edp) dedp \quad (3)$$

where IM_{ds} represents the capacity for damage state *ds* in terms of ground motion intensity (*IM*). The left-hand integrand in Equation 3 represents the probability that the ground motion intensity of interest, *im*, exceeds the capacity for the damage state, and can be computed using the distribution of

ground motion intensities causing a particular *edp* level. The right-hand integrand, $f\left(DST_{ds} = edp\right)$, can be computed using the defined damage state threshold information for the damage state. Note that $P\left(DST_{ds} \le edp\right)$ in Equation 2 is the cumulative distribution function (CDF) of DST_{ds}, while $f\left(DST_{ds} = edp\right)$ is the probability density function (PDF) of DST_{ds}. Equation 3 is useful due to practical difficulties in estimating $f\left(edp \mid im\right)$, mainly due to the fact that the *edp* is infinite or not available whenever *im* is larger than the collapse capacity intensity measure.

2.2 **Fragility for mainshock-damaged building**

The fragility for a mainshock-damaged building can be computed using Equation (4):

$$\begin{aligned} &P\left(DS_a > ds_a \mid IM_a = im_a, DS_m = ds_m\right) \\ &= \int P\left(DS_a > ds_a \mid IM_a = im_a, EDP_m = edp_m\right) \times f\left(EDP_m = edp_m \mid DS_m = ds_m\right) dedp_m \end{aligned} \quad (4)$$

where DS_a represents the post-aftershock damage state, DS_m represents the post-mainshock damage state, EDP_m represents the mainshock building response, and IM_a represents the ground motion intensity of an aftershock.

The first term in Equation 4, $P\left(DS_a > ds_a \mid IM_a = im_a, EDP_m = edp_m\right)$, can be computed using either Equation 1 or Equation 3 for a mainshock-damaged building whose mainshock response (EDP_m) is edp_m. The second term in Equation 4, $f\left(EDP_m = edp_m \mid DS_m = ds_m\right)$, can be computed using the assumed distribution of mainshock response given post-mainshock damage state. In reality, the integral over the continuous range of mainshock response is replaced with summation over discrete levels of mainshock response.

If we assume a deterministic mainshock response given the post-mainshock damage state, then

$$\begin{aligned} &P\left(DS_a > ds_a \mid IM_a = im_a, DS_m = ds_m\right) \\ &= P\left(DS_a > ds_a \mid IM_a = im_a, EDP_m = mDST_{ds,m}\right) \end{aligned} \quad (5)$$

where $mDST_{ds,m}$ is the mainshock response for the given post-mainshock damage state.

Furthermore, if we assume no uncertainty in the damage state threshold, then

$$\begin{aligned} &P\left(DS_a > ds_a \mid IM_a = im_a, DS_m = ds_m\right) \\ &= P\left(IM_{a,ds} < im_a \mid DST_{ds} = mDST_{ds,a}, EDP_m = mDST_{ds,m}\right) \end{aligned} \quad (6)$$

where $mDST_{ds,a}$ is the deterministic damage state threshold for post-aftershock damage.

3 **ILLUSTRATION**

For an illustration of the proposed methodology, we have developed fragilities for a typical mid-rise concrete moment resisting frame structure in New Zealand.

3.1 **Building simulation model**

For the numerical model, we chose a SDOF model that represents the typical mid-rise concrete moment resisting frame structure in New Zealand. The derivation of a multilinear capacity curve for the model is explained in detail in Ryu et al. (2008) and Uma et al. (2011). Figure 1 shows the capacity curve of the model along with the median damage state threshold for five damage states (Slight, Moderate, Extensive, Complete and Collapse). The logartithmic standard deviation of each damage state threshold was set to 0.4. To simulate the nonlinear hysteretic behavior of the model under dynamic loading, we assumed medium pinching ($\kappa_{f,d} = 0.5$) and medium levels of cyclic

deterioration ($\gamma_{s,a,d} = 50$ and $\gamma_k = 100$) (Ibarra, 2003). Figure 1b shows the hysteretic behavior of the model under cyclic static loading. The elastic damping ratio is 7%, chosen by taking the damping ratio of the midrise concrete moment frame (C1M) in the US-based HAZUS software (FEMA, 2003). The model has a vibration period of 1.3 seconds.

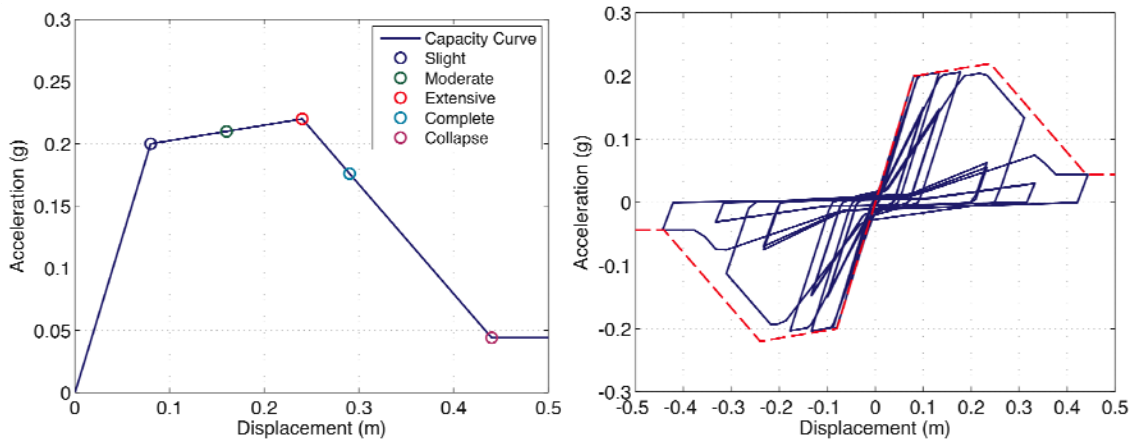

Figure 1 a) Capacity curve of the SDOF model; b) Hysteretic behavior of the model under static cyclic loading.

3.2 **Ground motions**

We used the suite of 30 records compiled by Vamvatsikos and Cornell (2006) for both mainshock and aftershock records. The moment magnitude for each of the records was within the range of 6.5 to 6.9, and the closest distance to fault rupture was within 15-33km. Spectral acceleration at 1.3 sec (i.e., the vibration period of the model) with a damping ratio of 5% was chosen as the ground motion intensity measure.

3.3 **Fragility of an undamaged building**

We performed IDA for a total of 30 mainshock records, and the resulting IDA curves are shown in Figure 2a. Using Equation 3, we computed the fragility of the undamaged building (i.e., the mainshock fragility) for each of the five damage states, including collapse, as shown in Figure 2b. The median and the logarithmic standard deviation of the collapse capacity of the undamaged building model are 0.86g and 0.42, respectively. Note that the *EDP* is the peak displacement of the SDOF model experienced during the earthquake.

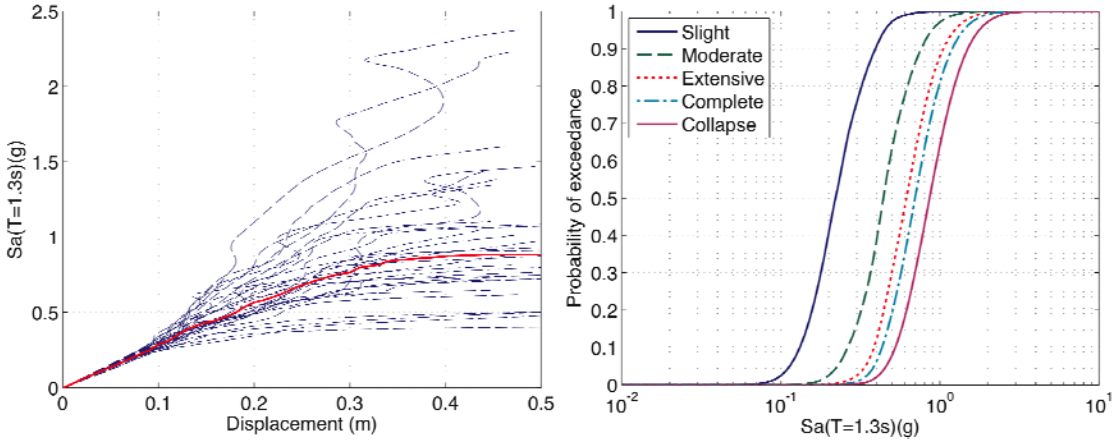

Figure 2 a) IDA curves for the undamaged building model; b) fragilities for the undamaged building model and the five potential damage states

3.4 **Simulation of mainshock damage**

In this paper, we focus on the collapse fragility (with respect to aftershocks) of the structure in the extensive damage state (due to a mainshock). The post-mainshock damage state is associated with the peak mainshock response. We have considered two different cases of a post-mainshock extensive damage state: 1) deterministic; the peak mainshock response is set equal to 0.24m, the median damage state threshold for the extensive damage state; 2) uncertain; the peak mainshock response is assumed to follow a lognormal distribution with 0.24m and 0.4 for the median and logarithmic standard deviation of the extensive damage state threshold, respectively.

In the case of the deterministic mainshock response, each mainshock record was scaled so that mainshock response was equal to 0.24m. In the case of the uncertain mainshock response, a similar approach may be applied; the process for the deterministic mainshock response was repeated for a number of sampled values representing the distribution of mainshock responses. Since it be too time-consuming to perform IDA for every possible value of mainshock response, we used Monte Carlo simulation instead, generating 30 values of mainshock response from the assumed distribution, and assigning each mainshock response to a mainshock record. Therefore the case of uncertain mainshock response is not different from the deterministic case in terms of computational effort.

3.5 **Performing IDA with a sequence of mainshock and aftershock records**

In order to perform IDA for a mainshock-damaged building, a sequence of mainshock and aftershock records was entered into the model. For a given sequence of mainshock and aftershock records, the scale factor for a given mainshock response was unchanged while the intensity of the aftershock record was scaled until the model collapsed.

Unlike the mainshock response, aftershock response can be different when the aftershock record is scaled by positive versus negative factors (to represent different polarities), because of residual drifts and damage in the mainshock-damaged building. In this study, we computed both aftershock responses by applying positive and negative factors to the aftershock records. Figure 3 shows two IDA curves where one is for the aftershock record scaled by positive factors and the other is for the aftershock record scaled by negative factors. Note that Luco et al. (2004) picked the smallest aftershock spectral acceleration that induced collapse for the residual collapse capacity. Similarly, we have used the polarity leading to the maximum aftershock response, as described below.

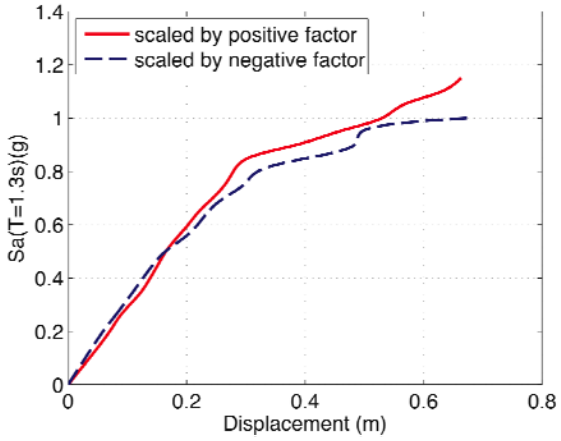

Figure 3 Comparison of two IDA curves: one is for an aftershock record scaled by positive factors, while the other is for an aftershock record scaled by negative factors.

The IDAs were performed using the OpenSees platform (McKenna and Fenves, 2000). Since IDAs over a sequence of mainshock and aftershock records require a large number of nonlinear dynamic analyses, the parallel version of OpenSees (OpenSeesMP) was run on a Linux cluster with multiple processors. The total number of dynamic analyses was the product of 30 (number of mainshock records), 30 (number of aftershock records), 2 (either positive or negative factors applied to aftershock

records), and the number of scale factors applied to each aftershock record until the model collapsed.

Figure 4a shows IDA curves for 30 sequences of various mainshock records and one aftershock record, whereas Figure 4b shows IDA curves for 30 sequences of one mainshock record and various aftershock records. As noted in Luco et al. (2004), there is relatively little variation with mainshock records of the aftershock response, since all the mainshock records are scaled to the considered level of mainshock response (in our case, for extensive damage).

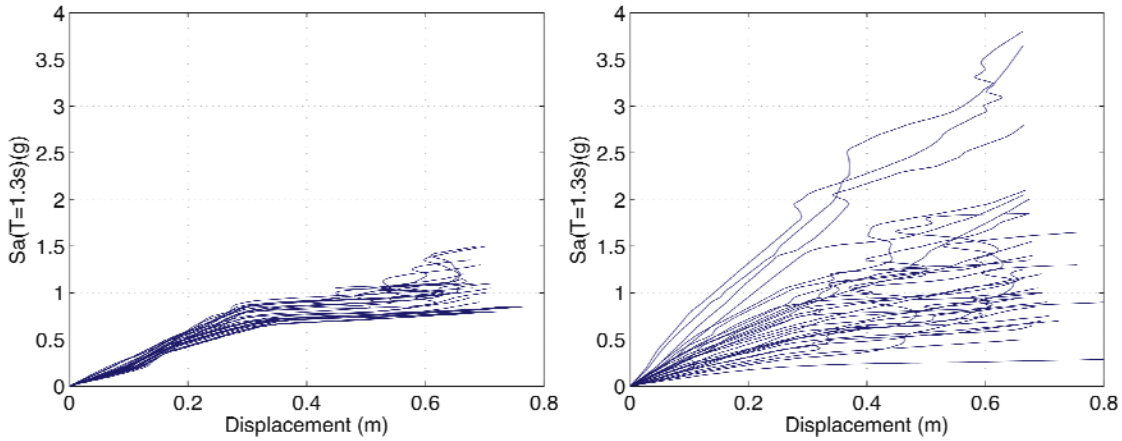

Figure 4 a) IDA curves for the sequences of various mainshock records and one aftershock record; b) IDA curves for the sequences of one mainshock record and various aftershock records.

3.6 **Fragility of mainshock-damaged building**

For the collapse damage state threshold, we have used either 1) a deterministic threshold, defined as 0.44m, the median damage state threshold for collapse, or 2) an uncertain threshold, defined by a lognormal distribution with 0.44m and 0.4 for the median and logarithmic standard deviation of the collapse damage state threshold, respectively.

First, we computed the collapse fragility of a mainshock-damaged building whose mainshock response was equal to a roof displacement 0.24m, using the deterministic collapse damage state threshold (see the Equation 5). Figure 5a shows three computed collapse fragility curves. As mentioned in the previous section, there were two aftershock responses depending on whether the aftershock record is scaled by positive or negative factors. In Figure 5a, the first curve was computed by choosing the maximum response between the positive and negative factors, the second curve was computed by choosing the minimum response between them, and the third curve was computed by choosing a response randomly between them. For this particular example, the differences among three cases are negligible. Hereafter, the collapse fragility computed using the maximum response will be used for comparison purpose.

Second, we computed the collapse fragility of a mainshock-damaged building whose mainshock response was equal to 0.24m, but with uncertainty in the 0.44m collapse threshold (see the Equation 4). The result is a negligible difference compared to the collapse fragility derived using the deterministic threshold, especially for lower levels of ground motion intensity.

Third, we computed the collapse fragility of a mainshock-damaged building whose mainshock response follows a lognormal distribution with 0.24m and 0.4 for the median and logarithmic standard deviation of the extensive damage state threshold, respectively, and with uncertainty in the collapse threshold (see the Equation 3).

All three of the computed collapse fragilities for a mainshock-damaged building are compared against the collapse fragility for the undamaged building in Figure 5b. The median collapse capacities of the mainshock-damaged building for three cases are 0.76g, 0.72g, and 0.72g, respectively. These represent decreases by approximately 16% from the median collapse capacity of 0.86g for the undamaged building. The reduction in the median collapse capacity is surprisingly small considering that the

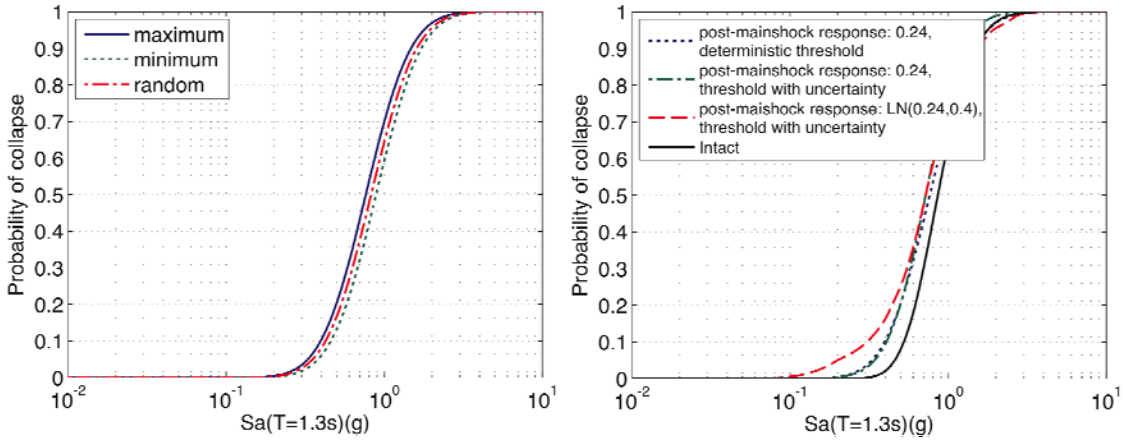

Figure 5 a) Comparison of three aftershock fragility curves depending on aftershock polarity; b) Comparison of three aftershock fragilities for a mainshock-damaged building against the collapse fragility for the undamaged (intact) building.

mainshock response corresponds to the extensive damage state, as also noted in Luco et al. (2004).

4 DISCUSSION

Figure 6a shows the median collapse capacity of the mainshock-damaged building versus mainshock response, using the deterministic mainshock response and deterministic threshold of collapse (see Equation 5). As alluded to in Section 3, the reduction in the median collapse capacity is small even for mainshock response beyond 0.29m, the median damage state threshold for complete damage. This surprising result is attributed to two observations. First, once the building experiences large nonlinear deformation, the characteristics of the damaged building, such as the fundamental period, change. Since the damaged model has a longer period, it might be less sensitive to the frequency content of an aftershock record than the undamaged or less-damaged building, as shown in Figure 6b. Second, the results depend on assumptions for cyclic deterioration and other nonlinear behavior. The cyclic deterioration model used in this study was not developed or verified for the simulation of nonlinear behavior of damaged buildings.

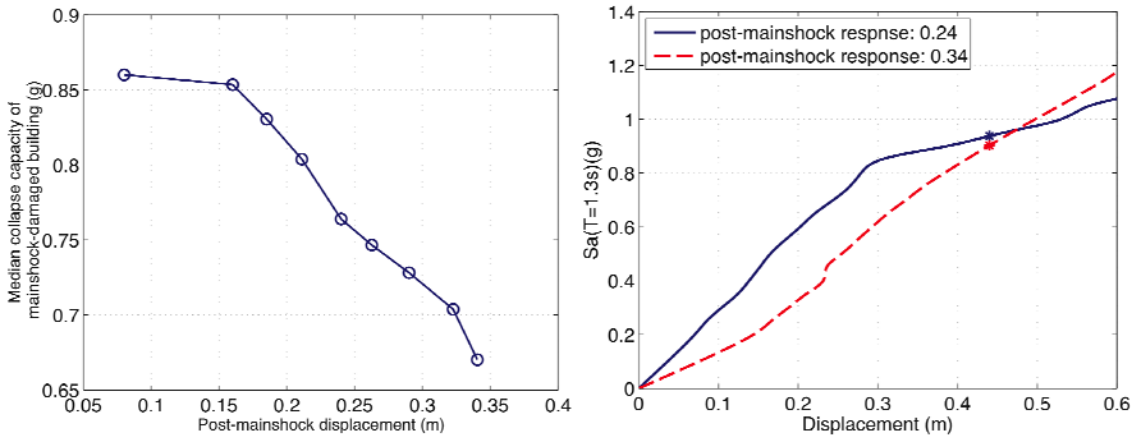

Figure 6 a) Median collapse capacity of mainshock-damaged building vs. mainshock response; b) Comparison of two aftershock IDA curves, whose post-mainshock responses are 0.24m and 0.34m, respectively.

Note that when we constructed IDA curves relating peak response to ground motion intensity, we only considered the building response due to the aftershock record, ignoring the peak mainshock response. As a result, the building has zero probability of collapse in low levels of aftershock ground motion intensity, as shown in Figure 5a and 5b. This was necessary for the purpose of computing damage

state transition probabilities, the probabilities of exceeding a higher damage state due to an aftershock, given a damage state caused by a mainshock. This should not be interpreted as ignoring mainshock damage in assessing post-aftershock damage states.

We also note that when selecting between two possible aftershock responses corresponding to the polarity of the aftershock record, it is more reasonable to select one randomly since it is unknown *a priori*; in other words, it is more reasonable to use the aftershock records as they are, which reduces the computational time by half.

5 SUMMARY

We present a methodology for developing fragilities for mainshock-damaged structures by performing incremental dynamic analysis (IDA) with a sequence of mainshock-aftershock ground motions. As an illustration of the methodology, we developed collapse fragilities for a typical New Zealand 5-storey reinforced concrete moment frame building, both undamaged and mainshock-damaged. Major conceptual improvements were made compared to the methodology in Luco et al (2004). Firstly, the proposed methodology is able to take into account uncertainty in the mainshock response for a given post-mainshock damage state. Second, the proposed methodology is able to take into account uncertainty in damage state thresholds when deriving the aftershock fragility.

The computed collapse fragility of a mainshock-damaged building can be coupled with the aftershock ground motion hazard at the location of the building in order to compute daily probability of collapse in an aftershock (Luco et al., 2011). This information helps structural engineers to assess whether a damaged building can continue to be occupied after a mainshock.

6 ACKNOWLEDGEMENTS

The work described in this paper has been carried out as a part of an EQC project (10/592) funded by the EQC Biennial Grants Programme 2010.

REFERENCES:

Federal Emergency Management Agency (FEMA). 2003. HAZUS-MH MR-1 Technical Manual, Federal Emergency Management Agency, Washington, D.C., USA.

Ibarra, L.F. 2003. Global collapse of frames structures under seismic excitations. Ph.D. Thesis, Department of Civil and Environmental Engineering, Stanford University, Stanford, California, USA.

Luco, N., Bazzurro, P., Cornell, C.A. 2004. Dynamic versus static computation of the residual capacity of a mainshock-damaged building to withstand an aftershock. 13th World Conference on Earthquake Engineering, Vancouver, Canada. Paper no. 2405.

Luco, N., Gerstenberger, M., Ryu, H., Uma, S.R., Liel, A.B., and Raghunandan, M. 2011. A methodology for probabilistic post-earthquake risk assessment that accounts for aftershocks, 9PCEE Paper No. 210.

McKenna, F. and Fenves, G.L. 2000. An object-oriented software design for parallel structural analysis. Advanced Technology in Structural Engineering, Proceedings of Structures Congress 2000, ASCE.

Ryu, H., Luco, N., Baker, J.W. and Karaca, E. 2008. Converting HAZUS capacity curves to seismic hazard compatible building fragility functions: effect of hysteretic models. The 14th World Conference on Earthquake Engineering, October 12-17, Beijing, China.

Uma, S.R., Ryu, H., Luco, N., Liel, A.B., Raghunandan, M. 2011. Comparison of main-shock and aftershock fragility curves developed for New Zealand and US buildings, 9PCEE Paper No. 227.

Vamvatsikos, D. and Cornell, C.A. 2006. Direct estimation of the seismic demand and capacity of oscillators with multi-linear static pushovers through IDA. Earthquake Engineering and Structural Dynamics, 35, pp.1097-1117.